

## Research Article





MOF-Based Dual-Layer Pickering Emulsion Very Important Paper

How to cite: Angew. Chem. Int. Ed. 2025, 64, e202421341 doi.org/10.1002/anie.202421341

# **MOF-Based Dual-Layer Pickering Emulsion: Molecular-Level Gating** of Water Delivery at Water-Oil Interface for Efficient Photocatalytic Hydrogenation Using H<sub>2</sub>O as a Hydrogen Source

Kuo Yuan<sup>+</sup>,\* Ying Zhang<sup>+</sup>, Zhuang Yan<sup>+</sup>, Qinbai Yun, Tiangun Song, Jun Guo, Jie Feng, Zheng Chen, Xiaotao Zhang, Zhiyong Tang, Wenping Hu, and Tongbu Lu\*

Abstract: Biphasic system not only presents a promising opportunity for complex catalytic processes, but also is a grand challenge in efficient tandem reactions. As an emerging solar-to-chemical conversion, the visible-light-driven and waterdonating hydrogenation combines the sustainability of photocatalysis and economic-value of hydrogenation. However, the key and challenging point is to couple water-soluble photocatalytic hydrogen evolution reaction (HER) with oilsoluble hydrogenation. Herein, we employed metal-organic frameworks (MOFs) and CdS nanorods to construct a MOF-CdS dual-layer Pickering emulsion (water in oil, W/O), which compartmented aqueous phase for photocatalytic HER and oil phase for hydrogenation. The hydrophobic MOF and hydrophilic CdS were isolated at the inner and outer layers of W/O emulsion, respectively. The molecularly regulated hydrophobicity of MOF controlled the water delivery onto CdS photocatalysts, which realized the synergistic regulation of HER and hydrogenation. In the photocatalytic hydrogenation of cinnamaldehyde, the highest yield of MOF-CdS Pickering emulsion reached 187.37 mmol·g<sup>-1</sup>·h<sup>-1</sup>, 30 times that of the counterpart without emulsion (6.44 mmol·g<sup>-1</sup>·h<sup>-1</sup>). Its apparent quantum yield reached 43.24 % without co-catalysts. To our knowledge, this performance is at a top-level so far. Our work realized the precise regulation of water-oil interface to effectively couple two reactions in different phases, providing new perspective for challenging tandem catalysis.

#### Introduction

As one of the most common phenomena in nature, the water-oil phase separation frequently occurs in human activities and hence palys an important role in daily life and production process. [1] From both practical and academic perspectives, the corresponding in-depth study and appropriate utilization are of great significance. [2] Especially in the field of catalysis, biphasic systems possess huge potential in complex catalytic processes, in which the clear compartment of water and oil is beneficial for tandem reactions (Scheme 1).[3] The two phases are connected via a water-oil interface, and hence the controllable mass transfer at interface is crucial for improving the whole catalytic performance of tandem reactions.<sup>[4]</sup> When photocatalytic and thermalcatalytic reactions are coupled together in the water-oil biphasic system, the sustainability and increasing economic value can be both realized in an as-designed tandem reaction.

As an important chemical reaction, hydrogenation is employed to synthesize intermediates for fine chemicals in perfume, flavouring, pharmacy and petrochemical industries.<sup>[5]</sup> In thermo-catalytic hydrogenation reactions (Figure 1), the elevated temperature, high pressure of H<sub>2</sub> and purification of complicated products all cause high cost, huge energy consumption and massive CO<sub>2</sub> emission.<sup>[6]</sup> Besides, the transportation, storage and usage of explosive H<sub>2</sub> gas further aggregate the safety risks during hydrogenation process.<sup>[7]</sup> Facing these grand challenges, tremendous efforts have been devoted to developing highly

[\*] Prof. Dr. K. Yuan, Y. Zhang, Dr. T. Song, J. Feng, Prof. Dr. T. Lu Institute for New Energy Materials and Low Carbon Technologies, School of Materials Science & Engineering, Tianjin University of Technology, Tianjin 300384, P. R. China

E-mail: yuankuo@email.tjut.edu.cn tongbulu@tjut.edu.cn

Prof. Dr. K. Yuan, Dr. T. Song, Dr. Z. Chen, Prof. Dr. X. Zhang, Prof. Dr. W. Hu

Department of Chemistry, School of Science & Key Laboratory of Organic Integrated Circuits, Ministry of Education, Tianjin University, Tianjin 300072, P.R. China

Dr. Z. Yan. Prof. Dr. Z. Tang

CAS Key Laboratory of Nanosystem and Hierarchical Fabrication, National Center for Nanoscience and Technology, Beijing, 100190, P.R. China

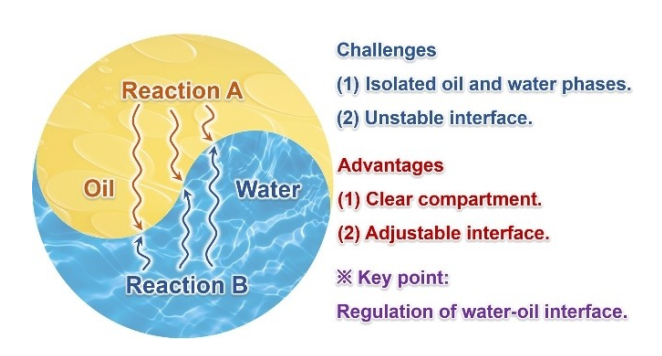
Prof. Dr. Q. Yun

Department of Chemical and Biological Engineering & Energy Institute, The Hong Kong University of Science and Technology, Kowloon, Hong Kong, China

State Key Laboratory of Separation Membranes and Membrane Processes, School of Chemistry, Tiangong University, Tianjin 300387, P.R. China

[+] These authors contributed equally to this work.





**Scheme 1.** The challenges, advantages and key points of water-oil phase separation.

efficient and selective catalysts to lower the reaction temperature or pressure of  $H_2$ . However, the explosion risk of  $H_2$  is just relieved to some extent, but not completely solved. Therefore, it is urgent and significant to develop a kind of clean, safe and easy-to-handle hydrogen source for hydrogenation.

Solid or liquid phase hydrogen possesses more stable physicochemical properties than H<sub>2</sub> gas but is extremely difficult to obtain under room temperature and atmospheric pressure.<sup>[9]</sup> Via forming hydrogen-storage chemicals (e.g., NaBH<sub>4</sub>, NH<sub>3</sub>BH<sub>3</sub>), these "solid or liquid" hydrogen sources not only maintain partial properties of H<sub>2</sub> but also reduce the explosion risk, which has been employed to replace H<sub>2</sub> gas in some specific fields, such as space fuel, propellant, hydrogenation and others. [10] However, the expensive cost, toxicity and pollution risk of hydrogen-storage chemicals impede their further large-scale applications.[11] In contrast, as one of the most abundant natural sources on the earth, H<sub>2</sub>O is regarded as an abundant, clean, safe and easy-tohandle hydrogen source.<sup>[12]</sup> Nevertheless, due to its inertial property, the thermo-catalytic water-donating hydrogenation still suffers from the high reaction temperature similar to other hydrogen-transfer reactions. [13] Given that  $H_2$  can be obtained from  $H_2O$  via electro- or photo-catalysis under room temperature, coupling the hydrogen evolution reaction (HER) with hydrogenation is able to address these challenges. [14]

Owing to the sustainability of solar energy, visible-lightdriven and water-donating hydrogenation is an appealing candidate for energy-saving and eco-friendly hydrogenation reactions. [15] To pursue excellent photocatalytic performance, the crucial issue is to efficiently couple photocatalytic HER with hydrogenation reaction. HER is usually performed in aqueous solution, and its performance is highly dependent on H<sub>2</sub>O delivery.<sup>[16]</sup> In contrast, most of hydrogenation substrates (e.g., unsaturated aldehydes, alkene, alkyne and so on) are oil-soluble and dissolved in oil-phase solution.[17] Given that water and oil are immiscible, these two reactions are separated into water and oil phases, and hence their coupling process is extremely challenging, which is a huge obstacle to improving the whole performance. In general, the bulk water and oil solution are separated into two phases by different densities in the vertical direction or by membrane catalysts, and the as-formed bulk oil-water interface acts as the only catalysis platform. [18] However, not only is the limited interface area unfavorable for efficient catalysis, [18b] but the fluctuating oil-water interface is also detrimental to the stable distribution of photocatalysts.<sup>[19]</sup> Hence, these issues make it a great challenge to optimize the oil-water interface catalysis performance.

For efficiently coupling the reactions in two phases, it is an urgent and significant issue to control and stabilize the oil-water interface. Owing to the vast interface area, emulsion solution might be an optimal candidate. As for the surfactant-based emulsion, amphiphilic molecules adsorb and desorb in a dynamic manner, causing the instability of interface. Whereas, nano- and micro-particles can be irreversibly stabilized at the oil-water interface (well-known as Pickering emulsions). [21] *Via* the sequential introduction

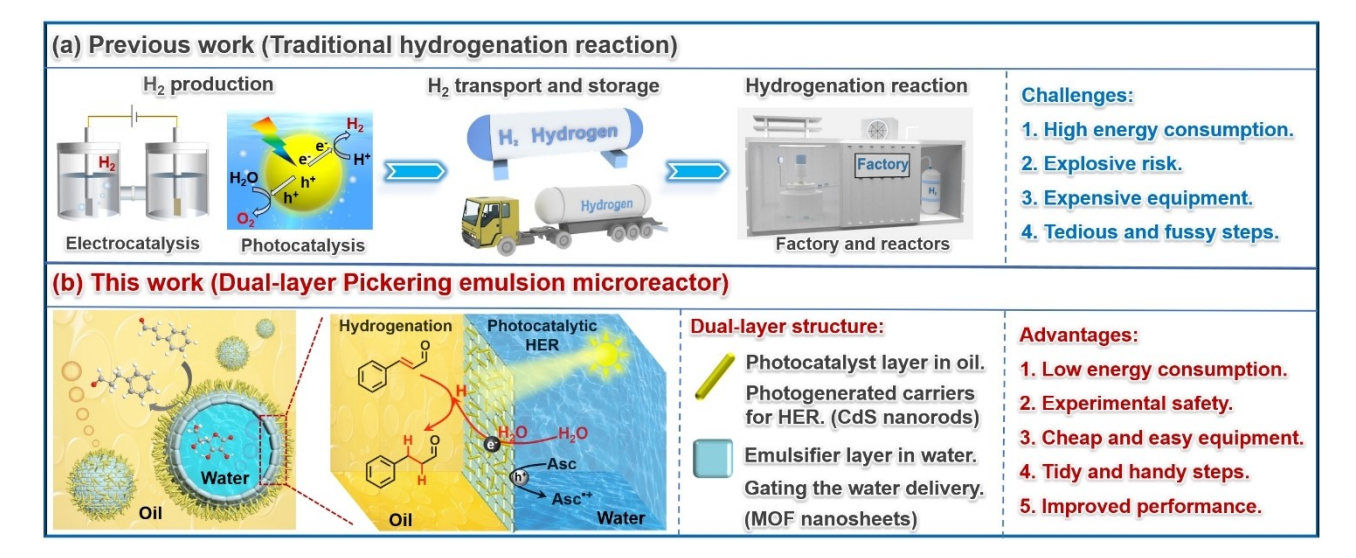


Figure 1. (a) Schematic diagrams of traditional hydrogenation reaction process containing H<sub>2</sub> production, H<sub>2</sub> transport and storage and hydrogenation reaction. (b) Dual-layer Pickering emulsion microreactor for coupling photocatalytic HER and hydrogenation reaction.



of colloidal materials, mixed-layer, dual-layer and multilayer Pickering emulsions can be ingeniously designed and constructed to cater numerous demands for challenging and complicated catalytic systems.<sup>[22]</sup> Among various emulsifier materials, metal–organic frameworks (MOFs) not only possess periodic channel structures, but also combine the advantages of inorganic and organic materials.<sup>[23]</sup> Multitudinous MOF-based composites have been reported and shown huge potential in catalytic fields.<sup>[24]</sup> Hence, MOFbased Pickering emulsion might be conductive to optimizing the photocatalytic hydrogenation performance using H<sub>2</sub>O as a hydrogen source.

In this work, we employed hydrophobic MOF emulsifier and hydrophilic CdS nanorod photocatalyst to construct MOF-CdS dual-layer Pickering emulsion (water in oil, W/ O), in which MOF and CdS were immobilized at the inner and outer shells of the emulsion, respectively (Figure 1b). As for the visible-light-driven water-donating hydrogenation reaction, the key point is to efficiently couple photocatalytic HER and hydrogenation reaction, which is closely related to the water layer coating around CdS. Trace water around CdS leads to the shortage of hydrogen source and hence is unfavorable for HER. In contrast, bulk water layer hinders the access of hydrogenation substrates to CdS, directly restraining hydrogenation process. Hence, only when the thickness of water layer is precisely regulated, can the performance for whole process be optimized to the maximum. In this MOF-CdS dual-layer Pickering emulsion, the hydrophobicity of MOF emulsifier could be molecularly regulated via decorating with different aliphatic acids, which played an important role in controlling the water delivery onto the surface of CdS. Briefly, CdS and MOF layers acted as the photocatalyst and gating role for water delivery, respectively (Figure 1b). In the photocatalytic measurements, the hydrogenation yield of CdS-MOF Pickering emulsion reached 187.37 mmol·g<sup>-1</sup>·h<sup>-1</sup>, 30 times as high as that of the counterpart without Pickering emulsion  $(6.44 \text{ mmol} \cdot \text{g}^{-1} \cdot \text{h}^{-1})$ . The apparent quantum yield reached 43.24% without co-catalysts. The experimental and calculation results both revealed that the unique structure of dual-layer Pickering emulsion is crucial for effectively coupling photocatalytic HER and hydrogenation reaction. This work offers a novel opportunity for visible-light-driven water-donating hydrogenation reactions and speeds up the further development of eco-friendly catalysis.

#### **Results and Discussion**

As a class of crystalline porous material, MOFs possess unique intrinsic properties and are widely employed in various fields. [23b] Besides, the excellent compatibility of MOFs with organic or inorganic materials enables the construction of various types of MOF-based composites for pursuing superior performance. Especially, MOF nanosheets, as a distinct type of 2D material, possess atomic-scale thickness, larger surface area, periodic porous structures and higher surface-to-volume atom ratios. [23a] Hence, MOF nanosheet is an appealing candidate as emulsifier for Pickering emulsion catalysts. Considering that the stability of emulsifier is quite important for the catalytic system, Zr-MOF nanosheets composed of zirconium and BTB (benzene-1,3,5-tribenzoate), i.e., Zr-BTB, were prepared as the emulsifier (Figure 2a). Via a post-synthetic modification (PSM) approach, ten kinds of aliphatic acids with different chain lengths (i.e., from formic acid to fencholic acid) were employed to further decorate the surface of Zr-BTB nanosheets, as shown in Figure 2a. According to the different chain lengths within aliphatic acids, these decorated Zr-BTB samples were labeled from C1-Zr-BTB to C10-Zr-BTB. As shown in Figures 2b, 2c and Figure S1, the transmission electron microscope (TEM), scanning transmission electron

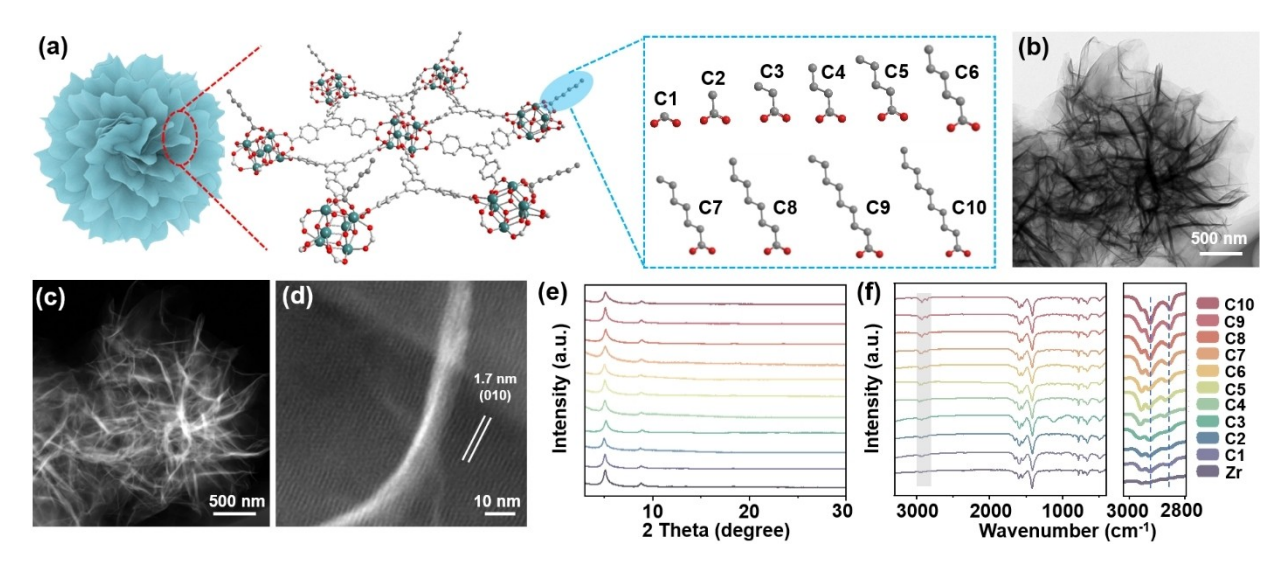


Figure 2. (a) The schematic diagram and crystal structure of Zr-BTB with different-chain fatty acids. Green, red and grey balls represented zirconium, oxygen and carbon atoms, respectively. (b-d) Bright-field TEM and dark-field STEM images of Zr-BTB nanosheets. XRD profiles (e) and FT-IR spectra (f) of Zr-BTB and C(1-10)-Zr-BTB nanosheets.



microscopy (STEM) and scanning electron microscope (SEM) images showed the nanosheet morphology of Zr-BTB. Similarly, the decorated C(1-10)-Zr-BTB samples also possessed nanosheet morphologies (Figures S2–S21). According to atomic force microscopy (AFM) characterization results, the thickness of original Zr-BTB or decorated C(1-10)-Zr-BTB was around 5.0 nm (Figures S22–S32). As shown in Figure. 2d, the HRTEM image of Zr-BTB nanosheet clearly showed the lattice fringe (1.7 nm) on the surface of nanosheets, corresponding to (010) crystal facet. Meanwhile, the XRD profiles of original Zr-BTB and C(1-10)-Zr-BTB samples were also consistent with the previous report, [19a] confirming their crystal structures (Figure 2e). These results all demonstrated the successful preparation of crystalline MOF nanosheets with uniform thickness.

To certify the decoration of aliphatic acids, Fourier transform infrared (FT-IR) spectroscopy was employed to characterize and uncover the surface properties of these MOF nanosheets. As shown in Figure 2f, two new characteristic peaks at 2925 and 2854 cm<sup>-1</sup> could be clearly observed in the FT-IR spectra of decorated C(1-10)-Zr-BTB, which were identified as the asymmetric and symmetric stretching vibration of -CH2-, respectively. Besides, the intensities of these two peaks gradually increased from C1-Zr-BTB to C10-Zr-BTB and showed a positive correlation with the chain-length of aliphatic acids. These results further proved that the surface of original Zr-BTB had been decorated with different aliphatic acids. As for the physcial mixture of C5acid and Zr-BTB (i.e., C5+Zr-BTB), the unanchored C5acid on Zr clusters of Zr-BTB could be removed by rinsing process, which was proved by FT-IR spectra, TEM images and GC-MS results (Figures S33 and S34). Hence, C(1-10)acids were anchored on the Zr clusters via coordination bonds, rather than physcial mixture in as-prepared C(1-10)-

Zr-BTB samples. As expected, the water contact angles on C(1-10)-Zr-BTB nanosheets gradually became larger along with increasing the chain-lengths of aliphatic acids (Figures 3a, S35 and Table S1). Hence, the hydrophobicity of C(1-10)-Zr-BTB was successfully regulated at molecular scale by PSM approach. Then, Zr-BTB and C(1-10)-Zr-BTB nanosheets were dispersed in ethyl acetate (EA), followed by dropwise addition of a certain amount of water under vigorous stirring. For original Zr-BTB, there was no Pickering emulsion formed, and only a foam layer floated on the surface of EA (Figure S36). After the anchor of aliphatic acids onto Zr-BTB, the obvious Pickering emulsion could be formed in the mixture solution of EA and water (Figure 3b and Figure S37). After one year, C(1-10)-Zr-BTB based Pickering emulsions could also be maintained to some extent, indicating their stabilities (Figure S38). As shown in Figures 3c, 3d, S39-S48 and Table S2, the average diameters of C1-Zr-BTB (0.36 mm) and C2-Zr-BTB (0.37 mm) were obviously smaller than those of C(3-10)-Zr-BTB samples (0.44-0.50 mm). Then the Zr-BTB nanosheets were labeled by Rhodamine B, and the confocal laser scanning microscope (CLSM) images showed that C5-Zr-BTB was immobilized at the shell of W/O Pickering emulsion (Figures 3e and 3f). Based on these results, it was demonstrated that C(1-10)-Zr-BTB-based Pickering emulsions possessed excellent stability in the mixture solution of EA and water, demonstrating their huge potential in catalysis.

To couple photocatalytic HER and hydrogenation reaction, it is an effective approach to construct a MOF-based Pickering emulsion photocatalysis system (Figure 4a). The primary issue is selecting a proper and efficient photocatalyst. Among multitudinous semiconductor materials, CdS is a kind of classical and widely employed photocatalyst for HER. Owing to the large specific surface area and

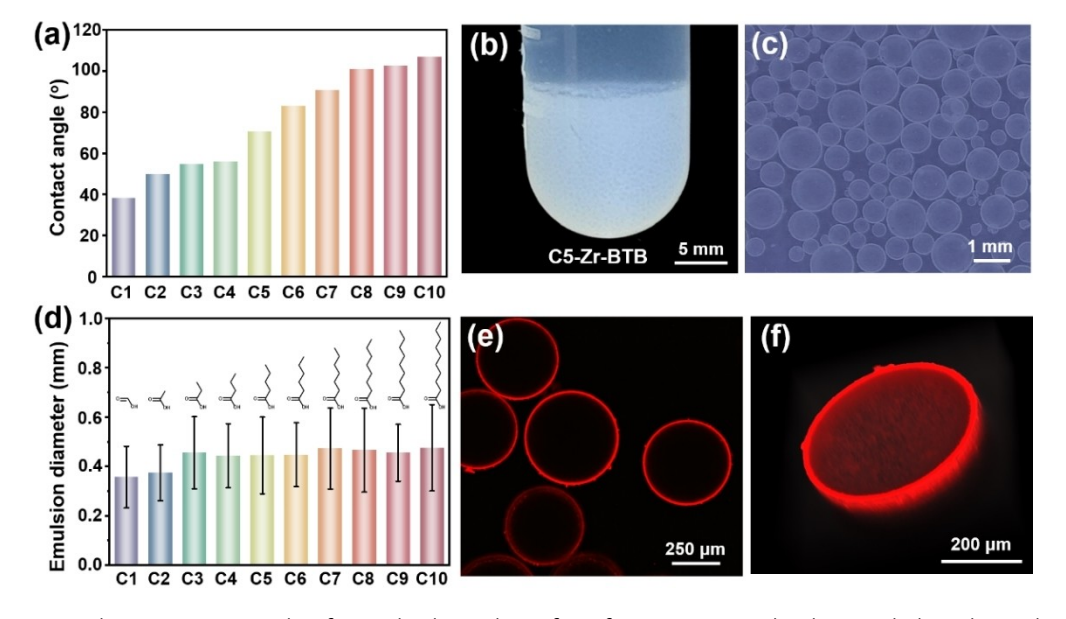


Figure 3. (a) Contact angle measurement results of water droplet on the surface of C(1-10)-Zr-BTB. The photograph (b) and optical image (c) of C5-Zr-BTB based Pickering emulsion. (d) Average diameters of C(1-10)-Zr-BTB-based Pickering emulsions. (e and f) CLSM image of C5-Zr-BTB-based Pickering emulsion.

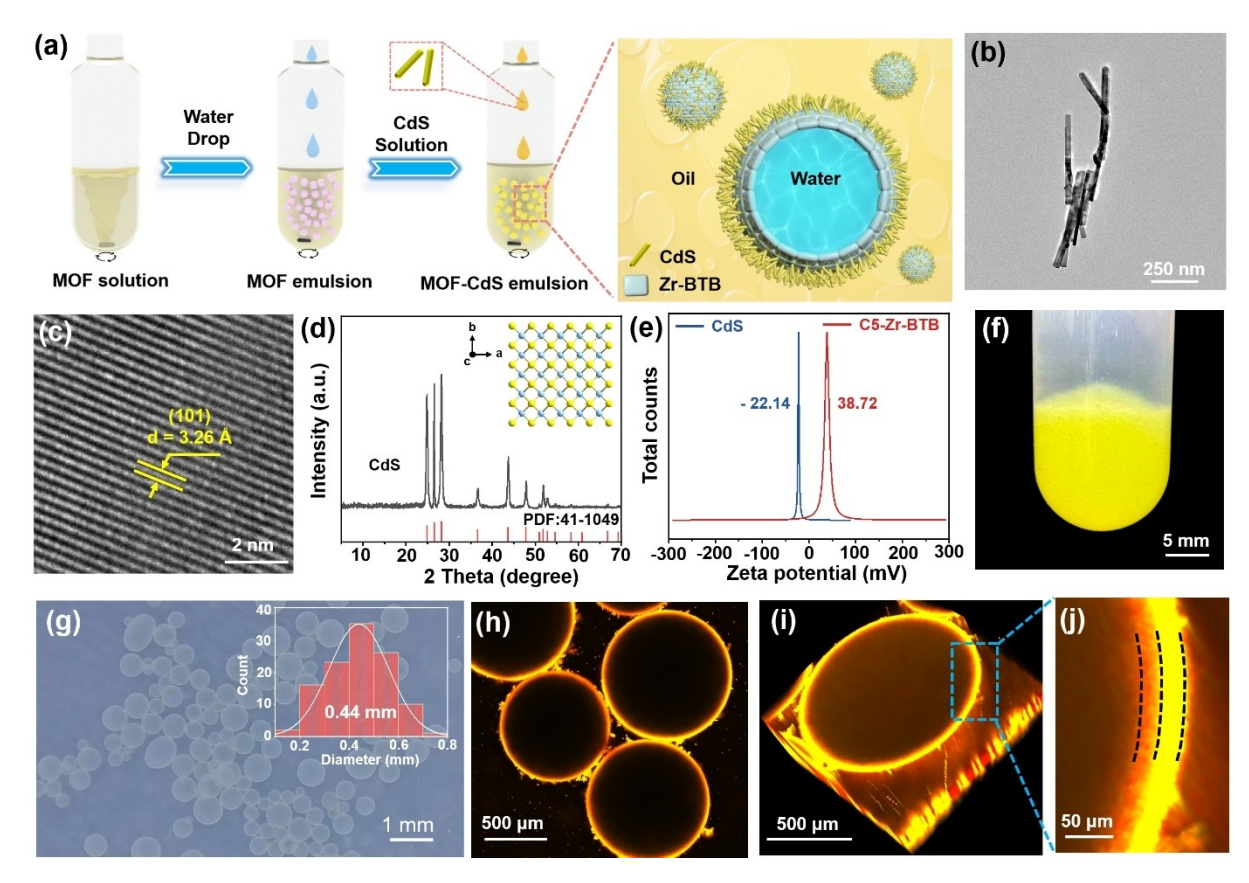


Figure 4. (a) Schematic diagram of constructing MOF-CdS dual-layer Pickering emulsion. (b and c) TEM and HRTEM images of CdS nanorods. (d) XRD profile and crystal structure (inset) of CdS nanorods. (e) Zeta potentials of CdS and C5-Zr-BTB. (f) Optical image of [C5-Zr-BTB]@CdS dual-layer Picker emulsion in a 10 mL centrifuge tube. (g) Optical image and corresponding size histogram (inset) of [C5-Zr-BTB]@CdS dual-layer Pickering emulsion. (h-j) CLSM images of [C5-Zr-BTB]@CdS dual-layer Pickering emulsion.

regulated band structures, CdS nanorods not only act as inorganic photosensitizers but also are widely employed to construct composites for photosynthesis. Via a solvothermal approach, CdS nanorods were synthesized, and their nanorod morphology was uncovered by TEM and SEM images (Figure 4b and Figure S49). Based on HRTEM image, the crystal lattice of CdS nanorods was around 3.26 Å, indexed to (101) crystal facet (Figure 4c). The XRD profile (Figure 4d) of as-obtained CdS nanorods was also consistent with the standard pattern (PDF: 41-1049), demonstrating its crystal structure. The water contact angle on the surface of CdS nanorods was only 18.3° (Figure S50), indicating its excellent hydrophilic property. Hence, the optimal water adsorption around CdS nanorods was kinetically favorable for photocatalytic HER. In addition, the CdS should be capable of photocatalyzing HER from a thermodynamic perspective, which was closely related to its light-absorbing capacity and band structure. As shown in Figure S51a, the UV/Vis spectra of CdS nanorods revealed their visible-light absorbing capacity of CdS. Based on the Tauc plot, the band gap of CdS was determined as 2.35 eV (Figure S51b). The Mott-Schottky result revealed that the conduction band of CdS was at -1.35 V, and the valence band was calculated as 1.19 V (Figures S51c and S51d). The electronic band structure and projected density of states (PDOS) of CdS were calculated using the Heyd-Scuseria-Ernzerhof (HSE06) hybrid functional within density functional theory (DFT), based on the slab models depicted in Figure S52. The calculations revealed that CdS exhibited a direct band gap of 2.53 eV, which was in close agreement with previously reported values and the experimental band gap of approximately 2.35 eV.<sup>[25]</sup> These consistent experimental and theoretical results both demonstrated that CdS nanorods could thermodynamically enable photocatalytic HER.

Given the kinetic and thermodynamic factors, the semiconductor CdS enabled photocatalytic hydrogenation. However, the photocatalytic activity was heavily dependent on the synergistic effect between photocatalytic HER and hydrogenation reaction, in which the key issue was to regulate the water layer adsorbing around CdS. For this purpose, CdS photocatalyst and MOF emulsifier should be employed to construct a type of Janus structure composites, i.e., dual-layer Pickering emulsion. As shown in Figure 4e, the zeta potential of CdS was -22.14 mV, opposite to that of C5-Zr-BTB (38.72 mV). Hence, via the electrostatic effect, CdS nanorods could be supported onto the surface of C5-Zr-BTB nanosheets. As shown in Figure 4a, C(1-10)-Zr-BTB was dispersed into EA solution, and then water was dropwise added to prepare C(1-10)-Zr-BTB one-layer Pickering emulsion. Following, the EA solution containing 5213773, 2025, 10, Downloaded from https://onlinelibrary.wiley.com/doi/10.1002/anie.202421341 by Tong-Bu La - Tianjin University Of, Wiley Online Library on [03/04/2025]. See the Terms and Conditions (https://onlinelibrary.wiley.com/terms-and-conditions) on Wiley Online Library or rules of use; OA articles are governed by the applicable Creative Commons I



CdS nanorods was added into the as-prepared one-layer Pickering emulsion solution to construct [C(1-10)-Zr-BTB]-CdS dual-layer Pickering emulsion. As shown in Figures 4f, 4g and Figure S53, the optical images showed that yellow Pickering emulsion with a diameter of 0.44 mm could be formed in EA solution and well maintained for two weeks. Its stability enabled the compartment of two reactions in aqueous and water phases. To distinguish different components in Pickering emulsion, C5-Zr-BTB and CdS were labelled by Rhodamine B and FITC-I dyes, respectively. As shown in CLSM images, two layers could be observed at the shell of W/O emulsion (Figures 4h-4j), revealing the dual-layer structure of [C5-Zr-BTB]@CdS Pickering emulsion. When more C5-Zr-BTB and less CdS were employed in dual-layer Pickering emulsion system, the red and yellow layers were more distinct (Figure S54). Besides, the SEM images showed that CdS nanorods were only isolated on the outer shell rather than inner shell (Figure S55). Based on these results, [C(1-10)-Zr-BTB]-CdS Pickering emulsion with the unique dual-layer structure and stability had been successfully prepared for the following photocatalytic hydrogenation reaction.

The hydrogenation of cinnamaldehyde was selected as the model reaction to be coupled with photocatalytic HER. The photocatalytic hydrogenation reaction was conducted in the as-prepared dual-layer Pickering emulsion system, and the details were clearly illuminated in Figure 5a. Water molecules could transfer through Zr-BTB layer to the surface of CdS and then be reduced to hydrogen for the following hydrogenation of cinnamaldehyde. Among the asprepared samples, [C5-Zr-BTB]-CdS realized the highest cinnamaldehyde conversion (79.61 %), as shown in Figure 5b and Table S3. The gas chromatography-mass spectrometry (GC-MS) results determined that benzenepropanal was the

main product (Figure S56). From C1-Zr-BTB to C5-Zr-BTB, the photocatalytic activity gradually increased. In contrast, further increasing the chain length of aliphatic acids, the conversion of cinnamaldehyde gradually decreased from 79.61% (C5-Zr-BTB) to 33.16% (C10-Zr-BTB). It was proved that C5-Zr-BTB was the best emulsifier for photocatalytic hydrogenation. As shown in Figure 5c and Table S4, single C5-Zr-BTB was not capable of photocatalyzing hydrogenation of cinnamaldehyde, demonstrating that CdS was the photocatalyst component. Hence, the photocatalytic mass activity based on CdS might be the proper parameter to evaluate the photocatalytic performance. The photocatalytic hydrogenation yield of [C5-Zr-BTB]-CdS reached 187.37 mmol·g<sup>-1</sup>·h<sup>-1</sup>, much higher than that of single CdS (6.44 mmol·g<sup>-1</sup>·h<sup>-1</sup>), indicating that the dual-layer structure in Pickering emulsion played an important role in improving photocatalytic performance (Figure 5c). Following, in dark or without ascorbic acid (AA), no product was detected, signifying that the light radiation and sacrificial agent were both necessary. Besides, the photocatalytic hydrogenation could not proceed in air, as the oxygen would participate in photocatalytic reduction, causing the inactivation of the whole photocatalytic process.41 By varying the adding amount of CdS, the Pickering emulsion could also form, and the diameter was around 0.43-0.44 mm (Figure 4g and Figure S57). When the adding amount of CdS was 150 µg, the hydrogenation yield reached the highest value (187.37 mmol·g<sup>-1</sup>·h<sup>-1</sup>), as shown in Figure 5d and Table S5. In order to verify the hydrogen source, H<sub>2</sub>O was replaced by D<sub>2</sub>O in the isotope trace experiment. As shown in Figure 5e, the m/z value of deuterium isotope labeled product was 136.1, and the m/z value of product was 134.1 in the common condition (i.e., H<sub>2</sub>O/ EA biphasic system). Hence, it was strongly confirmed that water was

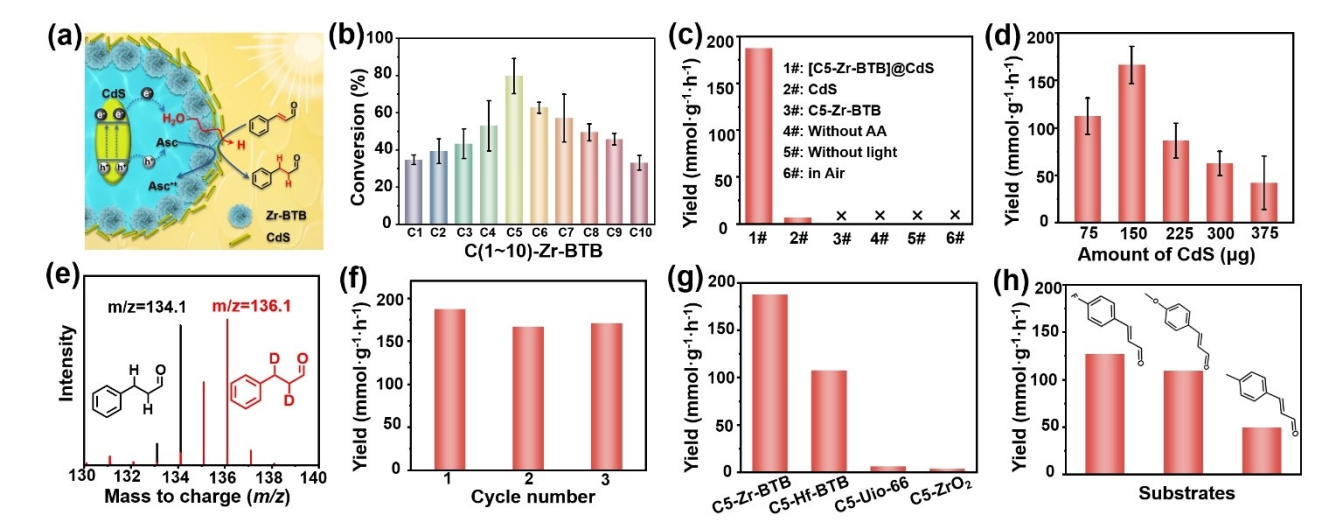


Figure 5. (a) Schematic diagram of photocatalytic hydrogenation of cinnamaldehyde using water as a hydrogen source in [Zr-BTB]@CdS dual-layer Pickering emulsion. (b) The conversion of cinnamaldehyde on [C(1-10)-Zr-BTB]@CdS in photocatalytic experiments. (c) Photocatalytic performances of [C5-Zr-BTB]@CdS and other controlled experiments. (d) Photocatalytic performances of [C5-Zr-BTB]@CdS with different amounts of CdS. (e) The MS spectra of normal photocatalytic hydrogenation reaction and the isotope labelling experiment with  $D_2O$  (m/z=20). (f) Cycling photocatalytic experiments of [C5-Zr-BTB]@CdS. (g) Photocatalytic performance of [C5-Zr-BTB]@CdS, [C5-Uio-66]@CdS and [C5-ZrO<sub>2</sub>]@CdS dual-layer Pickering emulsion. (h) Photocatalytic hydrogenation performance for different substrates.



indeed the hydrogen source participating in this photocatalytic reaction. After photocatalysis (2 hours), TEM images showed that CdS nanorods were supported on the surface of Zr-BTB nanosheets, and the corresponding elemental mapping revealed the uniform dispersion of Zr, Cd and S elements (Figure S58). Moreover, HRTEM image (Figure S59) showed that the crystalline fringe of CdS could also be maintained after 2-hour photocatalytic reaction, signifying the stability of crystalline CdS nanorods. In addition, as shown in Figure S60, the characteristic peaks of Zr-BTB could be observed in the XRD profile of used C5-Zr-BTB after photocatalysis (2 hours). These results demonstrated the excellent stability of MOF emulsifier and CdS photocatalyst. Following, the [C5-Zr-BTB]-CdS was employed in cycling experiments, and the yields of three cycles were 187.37, 166.95 and 170.95  $\text{mmol} \cdot \text{g}^{-1} \cdot \text{h}^{-1}$  without obvious decrease (Figure 5f and Table S6), indicating its promising application potential.

As the emulsifier, the regulation of superficial hydrophobicity was vital for the formation of Pickering emulsion. Fortunately, MOF nanosheets possess much larger specific surface area and higher surface-to-volume atom ratios, compared with MOF nanoparticles and traditional metal oxides. Hence, more aliphatic acids could be decorated on MOF nanosheets, which guaranteed the more feasible and thorough regulation on their surface hydrophobicity. To deeply investigate their advantages, Uio-66 nanoparticles and ZrO<sub>2</sub> powder were selected as the emulsifier materials for photocatalysis. Via a solvothermal approach, Uio-66 nanoparticles were synthesized. TEM image and XRD profile revealed the octahedron morphology and crystalline structure of Uio-66 (Figures S61a-S61c). After decorating valeric acid, C5-Uio-66 could still maintain original morphology and crystalline structure (Figures S62a and S62b), and the water contact angle increased from 32.3° to 87.7° (Figures S61d and S62c). The similar phenomena also occurred on the commercial ZrO<sub>2</sub> and C5-ZrO<sub>2</sub> samples (Figures S63 and S64). With the same molar amount of Zr element, C5-Uio-66 and C5-ZrO<sub>2</sub> were employed as emulsifiers in the photocatalytic system, but no Pickering emulsion was formed in the mixed solution of water and EA (Figures S62d and S64d). The photocatalytic hydrogenation yields of C5-Uio-66- and C5-ZrO2-based photocatalysts were just 6.27 and 3.99 mmol·g<sup>-1</sup>·h<sup>-1</sup>, respectively (Figure 5g and Table S7), much lower than that of [C5-Zr-BTB]-CdS (187.37 mmol·g<sup>-1</sup>·h<sup>-1</sup>). Hence, in comparison with MOF nanoparticles or traditional metal oxides, Zr-BTB nanosheets possessed unique superiority in Pickering emulsion catalysis. In order to verify the universality of this strategy, Hf-BTB and C5-Hf-BTB nanosheets were prepared, and TEM images clearly showed their nanosheet morphologies (Figure S65). As shown in Figure S65, the obvious crystalline fringes of Hf-BTB (1.7 nm) and C5-Hf-BTB (1.7 nm) could both be clearly observed in the HRTEM images, indicating their crystalline structures. In addition, the XRD curves of Hf-BTB and C5-Hf-BTB could both kept consistent with the previously reported result (Figure S66). [26] The water contact angle increased from 26.43° to 68.04° (Figure S67). The [C5-Hf-BTB]-CdS duallayer Pickering emulsion was successfully prepared (Figure S68), and its photocatalytic hydrogenation yield reached 107.74 mmol·g<sup>-1</sup>·h<sup>-1</sup>, much higher than those of [C5-Uio-66]-CdS (6.27 mmol·g<sup>-1</sup>·h<sup>-1</sup>) and [C5-ZrO2]-CdS (3.99 mmol·g<sup>-1</sup>·h<sup>-1</sup>), as shown in Figure 5g and Table S7. It was further demonstrated that the unique dual-layer structure of Pickering emulsion played an important role in improving the photocatalytic hydrogenation performance.

Then, [C5-Zr-BTB]-CdS dual-layer Pickering emulsion was employed in photocatalytic hydrogenation of other  $\alpha,\beta$ -unsaturated aldehydes, such as 4-fluorocinnamaldehyde, 4-methoxycinnamaldehyde and 3-methylcinnamaldehyde, and the corresponding yields reached 127.15, 108.98 and 49.00 mmol·g<sup>-1</sup>·h<sup>-1</sup>, respectively (Figure 5h, Scheme S1 and Table S8). The above results demonstrated that [C5-Zr-BTB]-CdS dual-layer Pickering emulsion system was an appropriate platform to couple photocatalytic HER and hydrogenation reaction.

The results of photocatalytic experimental results revealed that the formation of dual-layer Pickering emulsion was crucial for improving photocatalytic performance. To investigate catalytic mechanism, four controlled samples were prepared and tested in photocatalytic hydrogenation, as shown in Figure 6a. (i) CdS/[C5-Zr-BTB] one-layer Pickering emulsion was obtained in the mixture solution of EA and water (Figure S69a), and the synthetic details were illustrated in Figure S70. As shown in Figure S71, CLSM images demonstrated that the physical mixture of CdS and C5-Zr-BTB was immobilized at shell of W/O emulsion. (ii) CdS nanorods were added into the mixture solution of water and EA without Pickering emulsion (Figure S69b), and CdS nanorods were immobilized at the EA/water interface. (iii) The surface of CdS nanorods were decorated by valeric acids (Figures S72 and S73), and the as-obtained C5-CdS layer was imobilized at the EA-water interface without Pickering emulsion (Figure S70c). (iv) CdS and C5-Zr-BTB were dispersed into the mixed solution of CH<sub>3</sub>CN and H<sub>2</sub>O (v/v=4:1) without separation of water and oil (Figure S70d), i.e., CdS+[C5-Zr-BTB]. Then, the four controlled samples were employed in photocatalytic hydrogenation of cinnamaldehyde measurements. As shown in Figure 6b and Table S9, the photocatalytic yield of CdS/[C5one-layer Zr-BTB] Pickering emulsion 78.39 mmol·g<sup>-1</sup>·h<sup>-1</sup>, much lower than that of [C5-Zr-BTB]-CdS dual-layer Pickering emulsion (187.37 mmol·g<sup>-1</sup>·h<sup>-1</sup>), verifying the importance of dual-layer structure in optimizing photocatalytic performance. In the absence of C5-Zr-BTB, the yields of CdS and C5-CdS were only 6.44 and  $2.26 \text{ mmol} \cdot \text{g}^{-1} \cdot \text{h}^{-1}$ , respectively. In addition, when the EA and water biphasic solution was replaced by the one-phase solution (CH<sub>3</sub>CN and water), cinnamaldehyde could not be hydrogenated in this photocatalysis system. Besides, as for common surfacant-based emulsion (e.g., CTAB, CTAC, TBAC and SDBS), no photocatalytic hydrogenation product was detected, which ascribed to the unstable water-oil interface (Figures S74-S76). These results all proved that the dual-layer Pickering emulsion was crucial for efficient photocatalytic hydrogenation reaction.

Figure 6. (a) Schematic diagrams of different counterpart samples and (b) the corresponding photocatalytic performances. (c) The effect of water layer coating around CdS nanorods on regulating photocatalytic hydrogenation performance. (d) Adsorption enthalpy measurements of cinnamaldehyde for CdS (blue curve) and C5-Zr-BTB (red curve) versus injection numbers. (e) The theoretical calculation investigation for catalyzing routes of hydrogenation. Orange, dark blue, gray and light blue balls represented S, Cd, C and H atoms, respectively.

Based on the above results, it was preliminarily supposed that the water layer coating around CdS played an important role in optimizing photocatalytic performance (Figure 6c). As shown in Figure S50, the water contact angle of CdS was only 18.3°, indicating that water tended to adsorb on the surface of CdS. In the CH<sub>3</sub>CN/H<sub>2</sub>O solution, a thick water layer coating around CdS caused the sluggish mass transfer of cinnamaldehyde, which was also consistent with the inactive performance (Figures 6b and 6c). In the MOF-CdS dual-layer Pickering emulsion, the thickness of water layer could be decreased by enhancing the hydrophobicity of Zr-BTB emulsifier. Along with increasing the chain-length of aliphatic acids from C5-Zr-BTB to C10-Zr-BTB, the water contact angle increased from 70.5° to 106.7°, and the photocatalytic activity also gradually decreased (Table S3). The enhanced hydrophobicity of emulsifier would lower the thickness of water layer around CdS. The ultrathin or inconsecutive water layer around CdS was beneficial for the delivery of cinnamaldehyde but caused the shortage of hydrogen source (Figure 6c), which was also in consistence with the decreased photocatalytic activity. In addition, by increasing the amount of C5-Zr-BTB, the diameter of Pickering emulsion decreased from 0.44 to 0.30 to 0.25 mm (Figure S77), and the photocatalytic hydrogenation yields decreased from 187.37 to 170.50 to 127.83 mmol·g $^{-1}$ ·h $^{-1}$ , as shown in Figure S78 and Table S10. The thicker C5-Zr-BTB emulsifier layer would lead to the less water access to CdS. The decreased amount of hydrogen source lowered the photocatalytic activity. Hence, it was also demonstrated that the proper amount of water around CdS was crucial for the coupling efficiency of photocatalytic HER and hydrogenation reaction. As an important evaluation factor, apparent quantum yield (AQY) should also be characterized. The AQY of [C5-Zr-BTB]@CdS reached 43.24% (Table S12), which was much higher than that of CdS for HER (5.78%). Hence, it was further certified the superiority of dual-layer

Pickering emulsion. In comparison with those photocatalyst for HER, [C5-Zr-BTB]@CdS in photocatalytic hydrogenation showed the top-level activity by weight and AQY value (Tables S13 and S14). Besides, as for photocatalyst in hydrogenation, this unique dual-layer Pickering emulsion showed significant advantage over activity and AQY. It was worth mentioned that the excellent photocatalytic performance in our work was only dependent on regulating water and oil environments around CdS, and no other co-catalyst was introduced, which was different from previously reported strategies.

Following, the photocatalytic hydrogenation process was further studied, in which the photocatalytic HER provided a hydrogen source for the following hydrogenation reaction. Hence, the photocatalytic HER on CdS nanorods should be firstly studied. In photocatalytic HER measurements, the H<sub>2</sub> yield of single CdS was just 19.61 μmol·g<sup>-1</sup>·h<sup>-1</sup>, Figure S79 and Table S11. After using Pt as co-catalysts, the H<sub>2</sub> yield reached 1633.26 μmol·g<sup>-1</sup>·h<sup>-1</sup> (Figure S80). These results manifested that CdS nanorods were capable of reducing proton to hydrogen, and the release of adsorbed \*H on CdS was difficult in the absence of Pt. Based on the in situ electron paramagnetic resonance (EPR) spectra of CdS, the appearance of DMPO- H characteristic peaks and decrease of TEMPO characteristic peak intensity both demonstrated the generation of \*H on CdS nanorods (Figure S81).<sup>[27]</sup> The adsorption energy of \*H on the S site (0.89 eV) was significantly lower than that on the Cd site (1.95 eV), indicating a stronger affinity of the S site for \*H adsorption (Figure S82). Moreover, as shown in Figure S83, the twodimensional charge density contour plots of CdS and CdS-H revealed that electron accumulation occurred at the adsorbed hydrogen atom, resulting in electron depletion at the neighboring Cd site after \*H adsorption. As for the following hydrogenation process. the adsorption enthalpies  $(\Delta H)$  of cinnamaldehyde on the CdS and C5-ZrBTB were 15213773, 2025, 10, Downloaded from https://onlinelibrary.wiley.com/doi/10.1002/anie.202421341 by Tong-Bu Lu - Tianjin University Of, Wiley Online Library on [03/04/2025]. See the Terms and Conditions (https://onlinelibrary.wiley.com/terms-and-conditions) on Wiley Online Library for rules of use; OA articles are governed by the applicable Creative Commons License

measured. As shown in Figure 6d and Figure S84, the  $\Delta H$  of C5-Zr-BTB reached 24.47 kcal mol<sup>-1</sup>, but the  $\Delta H$  of CdS was 0 kcalmol<sup>-1</sup>. Due to an exothermic process, C5-Zr-BTB played an important role in gathering cinnamaldehyde molecules around CdS for further hydrogenation. As shown in Figures 6e and S85-S87, DFT calculations were conducted to investigate the reaction mechanism of hydrogenation of cinnamaldehyde. The calculated free energy changes for the hydrogenation of the C=C and C=O bonds over CdS-2H were -2.68 eV and -2.19 eV with energy barriers of 0.05 eVand 1.33 eV, respectively. These results indicated that the hydrogenation of the C=C bond to form benzenepropanal was thermodynamically and kinetically favorable. In summary, CdS nanorods were capable of photocatalyzing the hydrogenation of cinnamaldehyde to obtain benzenepropanal from both thermodynamic and kinetic perspectives.

Additionally, when the Pt as cocatalyst were supported on the surface of CdS (i.e., CdS/Pt), the  $\rm H_2$  yield of [C5-Zr-BTB]-[CdS/Pt] reached 25.79 mmol·g<sup>-1</sup>·h<sup>-1</sup>, but no hydrogenation product was detected (Figures S88–S90 and Table S15). Pt as cocatalys accelerated the photocatalytic HER, causing that no \*H species was employed for hydrogenation. Hence, the synergistic regulation of HER and hydrogenation reaction was the key point for improving the photocatalytic hydrogenation performance. It was indirectly proved the significant role of the dual-layer Pickering emulsion structure.

To sum up, the [C5-Zr-BTB]-CdS dual-layer Pickering emulsion serves as an ideal platform for effectively coupling the photocatalytic hydrogen evolution reaction (HER) with the hydrogenation reaction, in terms of reaction kinetics.

#### Conclusion

In this work, we designed and constructed a MOF-CdS duallayer Pickering emulsion, in which MOF emulsifier and CdS photocatalytst were immobilized at the inner and outer shells of W/O emulsion, respectively. In W/O Pickering emulsion, the hydrophobicity of MOF nanosheets, i.e., C(1-10)-Zr-BTB, could be molecularly regualted via PSM approach, which realized the precisely gating of water delivery at the water-oil interface (i.e., the amount of water around CdS). Hence, the photocatalytic HER in water phase and hydrogenation in oil phase could be efficiently coupled to realize an efficient visible-light-driven and water-donating hydrogenation reaction. In the photocatalytic hydrogenation of cinnamadelhyde using water as a hydrogen source, [C5-Zr-BTB]@CdS realized the highest hydrogenation yield  $(187.37 \text{ mmol} \cdot \text{g}^{-1} \cdot \text{h}^{-1})$ . Besides, the AQY value reached 43.24 % under monochromatic irradiation ( $\lambda$ =450 nm). In this novel and unique MOF-CdS dual-layer Pickering emulsion, the mass transfer at oil-water interface could be precisely regulated by the hydrophobic MOF layer, which was crucial to effetively couple photocatalytic HER with hydrogenation reaction. This work provides a novel insight for efficient light-driven water-donating hydrogenation reaction. As a proof-of-concept, the Pickering emulsion is an ingenious catalyzing platform to couple reactions of two phases, which further boosts the innovation of future catalysis.

## **Supporting Information**

The authors have cited additional references within the Supporting Information.

## Acknowledgements

This work was supported by the National Natural Science Foundation of China (22205162), National Key Research and Development Program of China (2022YFA1502902), Guangdong Basic and Applied Basic Research Foundation (Nos. 2023A1515110010 and 2024A1515012653). The authors thank Prof. Xubing Li for his valuable suggestions about CdS nanorods.

## **Conflict of Interest**

The authors declare no conflict of interest.

## **Data Availability Statement**

The data that support the findings of this study are available in the supplementary material of this article.

**Keywords:** Photocatalytic hydrogenation  $\cdot$  water-oil interface  $\cdot$  metal-organic framework  $\cdot$  Pickering emulsion  $\cdot$  biphasic system

- a) B. Wang, W. X. Liang, Z. G. Guo, W. M. Liu, *Chem. Soc. Rev.* 2015, 44, 336–361; b) S. Zhao, Y. K. Jiang, Y. C. Fu, W. Chen, Q. R. Zhang, L. L. He, C. X. Huang, Y. Liu, X. C. Zeng, Y. Chai, *Nat. Commun.* 2024, 15, 7423–7433; c) Y. R. Zhang, Z. W. Ye, C. C. Li, Q. L. Chen, W. Aljuhani, Y. M. Huang, X. Xu, C. F. Wu, S. E. J. Bell, Y. K. Xu, *Nat. Commun.* 2023, 14, 1392–1404.
- [2] a) Z. Y. Guo, H. F. Jiang, H. Wu, L. L. Zhang, S. Q. Song, Y. Chen, C. Y. Zheng, Y. X. Ren, R. Zhao, Y. H. Li, Y. Yin, M. D. Guiver, Z. Y. Jiang, *Angew. Chem. Int. Ed.* 2021, 60, 27078–27085; b) R. P. Hao, M. Zhang, D. P. Tian, F. Lei, Z. Q. Qin, T. Wu, H. Q. Yang, *J. Am. Chem. Soc.* 2023, 145, 20319–20327.
- [3] a) M. Zhang, R. Ettelaie, T. Yan, S. J. Zhang, F. Q. Cheng, B. P. Binks, H. Q. Yang, J. Am. Chem. Soc. 2017, 139, 17387–17396; b) M. P. Titus, L. Leclercq, J. M. Clacens, F. D. Campo, V. N. Rataj, Angew. Chem. Int. Ed. 2015, 54, 2006–2021; c) K. Piradashvili, E. M. Alexandrino, F. R. Wurm, K. Landfester, Chem. Rev. 2016, 116, 2141–2169.
- [4] a) Z. P. Wang, M. C. M. Oers, F. P. J. T. Rutjes, J. C. M. Hest, Angew. Chem. Int. Ed. 2012, 51, 10746–10750; b) Y. D. Duan, S. Z. Luo, Angew. Chem. 2024, 136, e202319206.
- [5] a) P. Gallezot, D. Richard, Catal. Rev. Sci. Eng. 1998, 40, 81–126;
   b) M. Luneau, S. L. Jin, D. A. Patel, C. H. Sykes, C. M. Friend, P. Sautet, Chem. Rev. 2020, 120, 12834–12872;
   c) L. L.





- Zhang, M. X. Zhou, A. Q. Wang, T. Zhang, *Chem. Rev.* **2020**, 120, 683–733
- [6] a) M. T. Zhao, K. Yuan, Y. Wang, G. D. Li, J. Guo, L. Gu, W. P. Hu, H. J. Zhao, Z. Y. Tang, *Nature* 2016, 539, 76–80;
  b) K. Yuan, T. Q. Song, D. W. Wang, X. T. Zhang, X. Gao, Y. Zou, H. L. Dong, Z. Y. Tang, W. P. Hu, *Angew. Chem. Int. Ed.* 2018, 130, 5810–5815.
- [7] C. N. Hinshelwood, G. H. Grant, Nature 1933, 131, 361-362.
- [8] a) P. X. Liu, Y. Zhao, R. X. Qin, S. G. Mo, G. X. Chen, L. Gu, D. M. Chevrier, P. Zhang, Q. Guo, D. D. Zang, B. H. Wu, G. Fu, N. F. Zheng, Science 2016, 352, 6287; b) A. J. Han, J. Zhang, W. M. Sun, W. X. Chen, S. L. Zhang, Y. H. Han, Q. C. Feng, L. R. Zheng, L. Gu, C. Chen, Q. Peng, D. S. Wang, Y. D. Li, Nat. Commun. 2019, 10, 3787; c) Y. Hu, M. Y. Liu, S. Bartling, H. Lund, H. Atia, P. J. Dyson, M. Beller, R. V. Jagadeesh, Sci. Adv. 2023, 9, 8225.
- [9] a) C. J. Pickard, R. J. Needs, Nat. Phys. 2007, 3, 473–476; b) B. Q. Cheng, G. Mazzola, C. J. Pickard, M. Ceriotti, Nature 2020, 585, 217–220; c) D. Berstad, S. Gardarsdottir, S. Roussanaly, M. Voldsund, Y. Ishimoto, P. Nekså, Renewable Sustainable Energy Rev. 2022, 154, 111772.
- [10] a) Y. Q. Guan, H. Wen, K. X. Cui, Q. R. Wang, W. B. Cao, Y. L. Cai, Z. B. Cheng, Q. J. Pei, Z. Li, H. J. Cao, T. He, J. P. Guo, P. Chen, *Nat. Chem.* 2024, 16, 373–379; b) A. Kumar, P. Daw, D. Milstein, *Chem. Rev.* 2022, 122, 385–441; c) S. Orimo, Y. Nakamori, J. R. Eliseo, A. Zuttel, C. M. Jensen, *Chem. Rev.* 2007, 107, 4111–4132.
- [11] a) M. S. Salman, C. Pratthana, Q. Lai, T. Wang, N. Rambhu-jun, K. Srivastava, K. F. Aguey-Zinsou, *Energy Technol.* 2022, 10, 2200433; b) Y. J. Huang, Y. H. Cheng, J. Y. Zhang, *Ind. Eng. Chem. Res.* 2021, 60, 2737–2771; c) C. G. Lang, Y. Jia, X. D. Yao, *Energy Storage Mater.* 2020, 26, 290–312.
- [12] a) U. Eberle, M. Felderhoff, F. Schüth, Angew. Chem. Int. Ed. 2009, 48, 6608–6630; b) H. Y. Yu, A. Díaz, X. Lu, B. H. Sun, Y. Ding, M. Koyama, J. Y. He, X. Zhou, A. Oudriss, X. Feaugas, Z. L. Zhang, Chem. Rev. 2024, 124, 6271–6392.
- [13] a) S. H. Guo, X. H. Li, J. Li, B. Q. Wei, Nat. Commun. 2021, 12, 1343; b) D. C. Wang, R. Chen, X. Zhu, D. D. Ye, Y. Yang, Y. X. Yu, J. W. Li, Y. X. Liu, H. Zhao, Q. Liao, J. Phys. Chem. Lett. 2022, 13, 1602–1608.
- [14] a) C. H. Han, J. Zenner, J. Johny, N. Kaeffer, A. Bordet, W. Leitner, Nat. Catal. 2022, 5, 1110–1119; b) C. H. Han, L. L. Du, M. Konarova, D. C. Qi, D. L. Phillips, J. S. Xu, ACS Catal. 2020, 10, 9227–9235; c) H. Z. Li, Y. Gao, Y. M. Wu, C. B. Liu, C. Q. Cheng, F. P. Chen, Y. M. Shi, B. Zhang, J. Am. Chem. Soc. 2022, 144, 19456–19465; d) W. R. Mcnamara, Z. J. Han, C. J. Yin, W. W. Brennessel, P. L. Holland, R. Eisenberg, PNAS 2012, 109, 39; e) R. S. Sherbo, A. Kurimoto, C. M. Brown, C. P. Berlinguette, J. Am. Chem. Soc. 2019, 141, 7815–7821
- [15] a) M. Q. Li, N. Zhang, R. Long, W. Ye, C. M. Wang, Y. J. Xiong, Small 2017, 13, 1604173; b) F. Arcudi, L. Đorđević, N. Schweitzer, S. I. Stupp, E. A. Weiss, Nat. Chem. 2022, 14, 1007–1012; c) R. Baba, S. Nakabayashi, A. Fujishima, K. Honda, J. Am. Chem. Soc. 1987, 109, 8.

- [16] a) A. A. Feidenhans'l, Y. N. Regmi, C. Wei, D. Xia, J. Kibsgaard, L. A. King, Chem. Rev. 2024, 124, 5617–5667; b) P. Verma, A. Singh, F. A. Rahimi, P. Sarkar, S. Nath, S. K. Pati, T. K. Maji, Nat. Commun. 2021, 12, 7313; c) Y. Q. Wang, Z. L. Qiao, H. Li, R. Zhang, Z. H. Xiang, D. P. Cao, S. T. Wang, Angew. Chem. Int. Ed. 2024, 63, e202404726.
- [17] a) K. Choe, F. B. Zheng, H. Wang, Y. Yuan, W. S. Zhao, G. X. Xue, X. Y. Qiu, M. Ri, X. H. Shi, Y. L. Wang, G. D. Li, Z. Y. Tang, Angew. Chem. 2020, 132, 3679–3686; b) G. Huang, Q. H. Yang, Q. Xu, S. H. Yu, H. L. Jiang, Angew. Chem. Int. Ed. 2016, 55, 7379–7383; c) J. Chun, S. Kang, N. Park, E. J. Park, X. Jin, K. D. Kim, H. O. Seo, S. M. Lee, H. J. Kim, W. H. Kwon, Y. K. Park, J. M. Kim, Y. D. Kim, S. U. Son, J. Am. Chem. Soc. 2014, 136, 6786–6789.
- [18] a) Y. Zhao, Y. Kondo, Y. Kuwahara, K. Mori, H. Yamashita, Appl. Catal. B 2024, 351, 123945; b) Y. Isaka, Y. Kawase, Y. Kuwahara, K. Mori, H. Yamashita, Angew. Chem. Int. Ed. 2019, 131, 5456–5460; c) W. G. Guo, X. H. Liu, Y. Liu, C. Li, ACS Catal. 2018, 8, 328–341.
- [19] a) K. Yuan, T. Q. Song, C. H. Yang, J. Guo, Q. H. Sun, Y. Zou, F. Jiao, L. J. Li, X. T. Zhang, H. L. Dong, L. Q. Li, W. P. Hu, J. Am. Chem. Soc. 2021, 143, 17526–17534; b) K. Yuan, K. Y. Tao, T. Q. Song, Y. Zhang, T. Zhang, F. Wang, S. M. Duan, Z. Chen, L. J. Li, X. T. Zhang, D. C. Zhong, Z. Y. Tang, T. B. Lu, W. P. Hu, J. Am. Chem. Soc. 2024, 146, 6893–6904.
- [20] W. Ramsden, Roy. Soc. Proc., vol. 1890, 48, 127-140.
- [21] a) C. H. Han, P. Meng, E. R. Waclawik, C. Zhang, X. H. Li, H. Q. Yang, M. Antonietti, J. S. Xu, *Angew. Chem. Int. Ed.* 2018, 57, 14857–14861; b) L. Ni, C. Yu, Q. B. Wei, D. M. Liu, J. S. Qiu, *Angew. Chem. Int. Ed.* 2022, 134, e202115885.
- [22] a) H. Wu, X. L. Du, X. H. Meng, D. Qiu, Y. Qiao, Nat. Commun. 2021, 12, 6113; b) A. Moreno, M. H. Sipponen, Nat. Commun. 2020, 11, 5599; c) D. C. Dewey, C. A. Strulson, D. N. Cacace, P. C. Bevilacqua, C. D. Keating, Nat. Commun. 2014, 5, 4670; d) K. Kim, S. Kim, J. Ryu, J. Jeon, S. G. Jang, H. Kim, D. G. Gweon, W. B. Im, Y. Han, H. Kim, S. Q. Choi, Nat. Commun. 2017, 8, 14305.
- [23] a) M. T. Zhao, Y. Huang, Y. W. Peng, Z. Q. Huang, Q. L. Ma, H. Zhang, *Chem. Soc. Rev.* **2018**, *47*, 6267; b) K. Jayaramulu, F. Geyer, A. Schneemann, Š. Kment, M. Otyepka, R. Zboril, D. Vollmer, R. A. Fischer, *Adv. Mater.* **2019**, *31*, 1900820.
- [24] D. P. Tian, R. P. Hao, X. M. Zhang, H. Shi, Y. W. Wang, L. F. Liang, H. C. Liu, H. Q. Yang, Nat. Commun. 2023, 14, 3226.
- [25] Q. Q. Mu, Y. H. Su, Z. H. Wei, H. Sun, Y. B. Lian, Y. Y. Dong, P. W. Qi, Z. Deng, Y. Peng, J. Cat. 2021, 397, 128.
- [26] L. Cao, Z. Lin, F. Peng, W. Wang, R. Huang, C. Wang, J. Yan, J. Liang, Z. Zhang, T. Zhang, L. Long, J. Sun, W. Lin, *Angew. Chem. Int. Ed.* 2016, 55, 4962–4966.
- [27] B. Yang, K. Liu, Y. Ma, J. J. Ma, Y. Y. Chen, M. Huang, C. Yang, Y. Hou, S. F. Hung, J. C. Yu, J. Zhang, X. Wang, Angew. Chem. Int. Ed. 2024, 63, e202410394.

Manuscript received: November 3, 2024 Accepted manuscript online: January 2, 2025 Version of record online: January 10, 2025